American Mineralogist, Volume 70, pages 1298–1308, 1985

Crystal structure refinement of anandite-2*Or*, a barium- and sulfur-bearing trioctahedral mica

MARLENE A. FILUT, AUDREY C. RULE, AND S. W. BAILEY

Department of Geology and Geophysics
University of Wisconsin, Madison, Wisconsin 53706

Abstract

The structure of anandite-2*Or*, ideally $BaFe_3^{2+}(Si_3Fe^{3+})O_{10}(OH)S$, has been refined to $R_w = 6.4\%$ using 1074 reflections. Unit cell parameters are $a = 5.439(1)$, $b = 9.509(2)$, and $c = 19.878(6)$Å. The symmetry is reduced from the ideal *Ccmm* to *Pnmn* as a result of ordering of tetrahedral Fe^{3+} and Si, octahedral Fe and Mg, and the anions OH and S. Mean bond lengths are T(1)–O = 1.620Å, T(2)–O = 1.799Å, M(1)–O,OH = 2.097Å, M(2)–O,S = 2.236Å, M(3)–O,S = 2.228Å, and M(4)–O,OH = 2.120Å. Sulfur, which substitutes for OH, is present as S^{2-} and moves by 0.16Å toward the interlayer Ba so that it serves as a 13th neighbor. This severely distorts the shapes of the Fe-rich *trans* M(2) and *cis* M(3) octahedra. Fe^{3+}-rich T(2) tetrahedra are linked to one another across the mirror plane, and small rings of four T(1) + two T(2) alternate with large rings of two T(1) + four T(2) in each tetrahedral sheet but are shifted to face one another in adjacent layers across the interlayer gap. The interlayer Ba moves deeper into the larger ring by 0.1Åalong **c** towards the sulfur.

The 6-fold rings are essentially hexagonal ($\alpha = 0.9°$). The usual instability of prismatic coordination around an interlayer cation resulting from anion-anion repulsion is counterbalanced in anandite-2*Or* because (1) the divalent charge on Ba offsets more of the unsatisfied charges on the basal oxygens than would a univalent cation, (2) attraction exists between Ba^{2+} and S^{2-}, (3) alternating-wave corrugations in the basal oxygen surfaces are in-phase and do not lead to abnormally short contacts across the interlayer gap, and (4) alternation of the ordering pattern across the interlayer gap pairs the basal oxygen unique to hybrid T(2) with that unique to pure Si T(1).

Several lines of evidence suggest the true symmetry is $P2_1$ (**a**-axis unique), but attempted refinement in that subgroup has not been successful.

Introduction

Anandite is a trioctahedral brittle mica that to date has been identified only from Wilagedera, Ceylon (now Sri Lanka), where it occurs as thin bands and lenses within a magnetite–barite–sulfide ore zone. The enclosing calc-schists and calc-gneisses of Precambrian age have been subjected to granulite grade metamorphism (Pattiaratchi, 1961). The simplified formula of anandite is $Ba(Fe,Mg)_3(Si,Fe^{3+})_4O_{10}(OH)S$, which is unique because of the substantial substitution of S^{2-} for $(OH)^{-1}$. The essential presence of structural sulfur was proven by the microprobe analyses of Lovering and Widdowson (1968) and by the first structural refinement by Giuseppetti and Tadini (1972). It is also confirmed in the present study.

Three polytypes of anandite have been recognized. The original description of the mineral by Pattiaratchi et al. (1967) listed a powder pattern that can only be indexed as $2M_1$. The structural refinement of Giuseppetti and Tadini (1972) was of the 2*Or* polytype, as is the present study, and this appears to be the dominant polytype. A refinement of a 1*M* polytype is also in progress (T. Kato, personal comm. to S. W. Bailey, 1984).

A second refinement of the 2*Or* structure has been carried out because of its unique nature and because of several inconsistencies in the original refinement. The structure is of special interest because of the structural S, interlayer Ba, and substantial tetrahedral Fe^{3+}. Ordering has reduced the symmetry from the ideal space group *Ccmm* to an apparent subgroup *Pnmn*. It is the only known mica in which *C*-centering of an orthohexagonal cell is violated and the only one in which ordered tetrahedral R^{3+} cations do not alternate with Si around each hexagonal ring. It is also the only mica for which the 2*Or* polytype has been verified. The refinement by Giuseppetti and Tadini (1972) was of only moderate accuracy, as indicated by the residual $R = 13.1\%$ for 853 reflections (only 409 observed) and by inconsistency between certain bond lengths and the composition. For example, tetrahedron T(1) was interpreted to be of composition $Si_{0.96}Al_{0.04}$ despite its mean bond length of 1.68Å. A more reasonable T–O bond would be 1.61–1.62Å for that composition. The mean T(2)–O bond of 1.77Å was interpreted to give a composition $Si_{0.36}Fe^{3+}_{0.35}Fe^{2+}_{0.29}$, and the possibility of tetrahedral Fe^{2+} is sufficiently unusual that it warrants further study. The present study confirms most of the major features of the Giuseppetti and Tadini structure,

clarifies the inconsistencies with a more accurate refinement, and uses the observed structural distortions and ordering pattern to explain the stability of the 2*Or* structure for this composition.

Experimental

A sample of the Wilagedera anandite was kindly sent to S. W. Bailey by Professor Th. G. Sahama of the University of Helsinki. About 35 platelets of different crystals were studied for perfection and symmetry by precession and Weissenberg methods. All of these crystals plus additional material ground up for a Debye-Scheerer pattern proved to be of the 2*Or* polytype. The powder pattern (Bailey, 1980) is quite different from that of the original $2M_1$ material.

A 2-layer periodicity evident on precession photographs in the *h*0*l* reflections and others with $k = 3n$ indicates the periodicity of the octahedral cations along **c**. They must alternate regularly in adjacent layers between the I and II sets of possible positions, thus restricting the polytype choices to 2*Or*, $2M_2$, or 6*H*. In any layer silicate there are three possible reciprocal **b*** or pseudo-**b*** axes, 60° apart in the plane normal to **c**, and three possible **a*** or pseudo-**a*** axes normal to the possible **b*** axes. Unfiltered precession photographs taken with the crystal mounted normal to (001) and with each possible **a** axis as the precession axis in turn (i.e., three photos taken 60° apart on the dial) can be used to determine true **b***, the cell shape, and its apparent symmetry. Determination of the true symmetry requires examination of a much larger number of reflection intensities. For these anandite crystals each of the three possible **b*** axes is observed to be normal to **c*** and to be outlined by white radiation streaks that extend continuously through the 0*k*0, *hh*0, or $h\bar{h}$0 reflections (as the case may be on the three photos) directly to the origin. The true **b*c*** photo is different from the two pseudo-**b*c*** photos in that it indicates only 1-layer periodicity along **c*** due to an apparent *n*-glide plane parallel to (100). These observations combine to indicate an orthogonal-shaped cell of apparent orthorhombic symmetry, thus the 2*Or* polytype with alternating intralayer shifts of $+a_1/3$ and $-a_1/3$.

A few reflections violating the systematic absences required by *C*-centering are evident on true **b*c*** and **a*c*** photos, and a large number on higher level photos. There are also violations of most of the other systematic extinctions required by *Ccmm* and *Pnmn* symmetry. It is clear that the structure can be approximated by *Pnmn*, however, because violations of the extinctions required by the *n*-glides and 2_1 screw axes are few in number. The structure has been refined as *Pnmn* for comparison with previous results. The possible true symmetry is discussed in a later section.

Electron microprobe analyses of three different grains showed little variation between or within grains. Table 1 lists the analysis obtained by courtesy of Dr. E. D. Glover by averaging four separate measurements, each obtained at eight different points, using an ARL microprobe model SEMQ as automated by Tracor Northern. Operating voltage was 15 kV and a current of 0.02 μA. The beam was focused at approximately 10 μm to avoid specimen damage. High purity oxides were used as standards for the major elements and wollastonite, jadeite, microcline (Asbestos, Quebec), rhodonite, scapolite, synthetic covellite, and fluorite were used for Ca, Na, K, Mn, Cl, S, and F, respectively. Corrections were made by the theoretical ZAF method. A Mössbauer analysis by courtesy of Dr. G. A. Waychunas of Stanford University indicated 45.6% of total Fe is present as Fe^{3+}. Only minor Mn is present, and the same ratio of 2+ : 3+ valences was assumed for Mn in the structural allocation as found for Fe.

Table 1. Allocation of microprobe analysis*

	wt. %	Atoms		
SiO_2	24.59(.58)	Si	2.599	4.000
FeO	41.73(.53)	Fe^{3+}	1.401	
Al_2O_3	0.80(.04)	Fe^{3+}	0.281	2.930
MgO	2.89(.12)	Fe^{2+}	2.006	
TiO_2	0.08(.02)	Al	0.099	
MnO	0.92(.02)	Mg	0.456	
BaO	23.05(.30)	Mn^{3+}	0.038	
K_2O	0.24(.01)	Mn^{2+}	0.044	
Na_2O	0.06(.02)	Ti	0.006	
CaO	0.00(.01)	Ba	0.955	1.000
S	4.25(.06)	K	0.032	
Cl	0.91(.06)	Na	0.013	
F	0.12(.01)	S	0.842	
Sum	99.64	Cl	0.163	
less O = S,Cl,F	2.38	F	0.040	
	97.26			

* Mössbauer analysis indicates 45.6% of total Fe is present as Fe^{3+}. Figures in parentheses indicate one standard deviation. Allocation assumes no vacancies in interlayer site, so Ba + K + Na = 1.0.

There is some question as to the correct method to allocate the analysis to a structural formula for anandite. The ideal formula assumes 23 positive and negative charges, but this is only true if there is exactly one S^{2-} anion per formula unit. The structural formula was derived initially by assuming an ideal 23 total positive charge on the cations and using the atomic ratios plus the assumption S + Cl = 1.0 to derive S, Cl, and F contents. The structural refinement later showed that the scattering power of the interlayer cation is essentially that of pure Ba, so that vacancies can be discounted. The final allocation shown in Table 1 uses the atomic ratios and the assumption Ba + K + Na = 1.0. The K + Na total is only 0.045 atoms. The differences between the initial and final allocations are minor. The Mössbauer analysis indicates 1.40 atoms of tetrahedral Fe^{3+} and no tetrahedral Fe^{2+}, identical with the allocation of Table 1.

The present analysis differs from the original wet chemical analysis of Pattiaratchi et al. (1967) in giving less FeO, Al_2O_3, TiO_2, CaO, and K_2O but more total Fe, Fe_2O_3, BaO, and S, plus the added elements Cl and F. Lovering and Widdowson (1968) found somewhat similar discrepancies with an electron microprobe analysis, and attributed the differences to biotite and augite contamination in the original sample. They reported the sulfur to be a primary constituent of the mineral, rather than due to pyrite impurity, and demonstrated that it was present as S^{2-} by measuring the wavelength shift of its S*K*α radiation. The present analysis is similar to that of Lovering and Widdowson but differs in showing less FeO, MnO, and Na_2O but more BaO, Fe_2O_3, S, and Cl, plus the added element F.

A triangular-shaped crystal, 0.7 mm on edge and 0.07 mm thick, was selected for detailed study. Unit cell dimensions of $a = 5.439(1)$, $b = 9.509(2)$, and $c = 19.878(6)$Å were determined by least-squares refinement of 15 high-angle reflections on a Syntex

Table 2. Final atomic coordinates and thermal parameters

Atom	x	y	z	B(eq)	β(11)	β(22)	β(33)	β(12)	β(13)	β(23)
Ba	0.6679(1)	0.0000	0.2553(0)	2.04	0.0167(2)	0.0091(1)	0.0005(0)	0.	0.0000(0)	0.
M(1)	0.0000	0.0000	0.0000	0.73	0.0069(6)	0.0023(2)	0.0004(0)	0.	0.0001(2)	0.
M(2)	0.5000	0.5000	0.0000	0.83	0.0095(4)	0.0022(1)	0.0004(0)	0.	-0.0003(1)	0.
M(3)	0.0000	0.6559(1)	0.0000	0.88	0.0064(3)	0.0038(1)	0.0003(0)	0.	0.0001(1)	0.
M(4)	0.5000	0.1690(1)	0.0000	0.80	0.0078(3)	0.0022(1)	0.0004(0)	0.	-0.0000(1)	0.
T(1)	0.1665(3)	0.1617(1)	0.1387(1)	0.69	0.0092(5)	0.0021(1)	0.0001(0)	-0.0000(2)	0.0000(1)	-0.0000(0)
T(2)	0.6701(2)	0.6667(1)	0.1403(1)	1.10	0.0098(3)	0.0044(1)	0.0003(0)	0.0002(1)	0.0000(1)	0.0002(0)
O(1)	0.1593(7)	0.1625(3)	0.0576(2)	0.75	0.0092(11)	0.0024(3)	0.0002(1)	-0.0000(5)	0.0004(3)	-0.0000(1)
O(2)	0.6762(7)	0.6688(3)	0.0506(2)	1.05	0.0060(10)	0.0029(3)	0.0009(1)	-0.0004(4)	0.0005(3)	0.0003(1)
O(3)	0.4124(9)	0.2293(5)	0.1706(2)	2.36	0.0188(16)	0.0100(5)	0.0008(1)	-0.0040(7)	-0.0017(3)	0.0003(2)
O(4)	0.9264(9)	0.7671(5)	0.1734(2)	2.16	0.0171(16)	0.0099(5)	0.0006(1)	-0.0040(7)	0.0016(3)	0.0004(2)
O(5)	0.1638(20)	0.0000	0.1656(3)	3.95	0.0868(58)	0.0027(5)	0.0004(1)	0.0	0.0000(8)	0.0
O(6)	0.6621(13)	0.5000	0.1811(3)	2.64	0.0178(22)	0.0127(9)	0.0008(1)	0.0	0.0002(6)	0.0
OH	0.6674(9)	0.0000	0.0509(3)	0.96	0.0051(13)	0.0	0.0	0.0	0.0	0.0
S	0.1665(3)	0.5000	0.0838(1)	1.88	0.0109(5)	0.0030(1)	0.0004(0)	0.0	-0.0001(1)	0.0
H+S	0.6709	0.0000	0.0903	2.000						

(Nicolet) $P2_1$ automated single crystal diffractometer. The intensities of 7357 reflections, 42% of which violate *C*-centering, were measured by the $\theta:2\theta$ variable scan mode over all eight octants of the limiting sphere out to 60° 2θ for monochromatic Mo$K\alpha$ radiation. Crystal and electronic stability were checked after every 50 reflections by monitoring a standard reflection, but no instability was found. Reflections were considered observed if the intensities were greater than 3.0 standard deviations. Integrated intensities were corrected for Lp effects and then for absorption by the empirical psi-scan method of North et al. (1968). The data were merged after correction into 1074 non-zero independent reflections consistent with *Pnmn* symmetry.[1]

Refinement

The atomic positions of Giuseppetti and Tadini (1972) were used as the starting coordinates for refinement by a modified ORFLS program. No cation ordering was assumed at the start, and hybrid scattering factor tables appropriate for the composition and for a 50% ionization state were calculated from the tables of Cromer and Mann (1968). Only the scale factor and atomic positions were varied at first, using fixed isotropic *B* values. When convergence was achieved, isotropic *B* values were added as variables to give a residual $R = 16.0\%$ with unit weights. At this stage the ordering pattern was evident from bond lengths, *B* values, and a difference electron density (DED) map. The scattering factor tables were revised accordingly to make T(1) 100% Si and T(2) a hybrid of composition $Fe^{3+}_{0.7}Si_{0.3}$. Octahedra M(2) and M(3) were made 100% Fe, and the small amounts of other octahedral cations present by analysis were distributed, along with Fe, over M(1) and M(4). Variations in the occupancies of the latter two sites were made during subsequent refinement. Anomalous scattering factors for Ba, Fe, Mg, S, and Si were constructed from data in the *International Tables for X-ray Crystallography*. Final refinements were made with both unit weights and sigma weights. In other layer silicate refinements made in this laboratory it was found that unit weights give both smaller *R* values and smaller positional errors, but this was not the case for anandite. Final convergence after varying all atomic coordinates and anisotropic temperature factors gave $R = 5.2\%$ with unit weights, but the positional errors determined by program ORFFE were considerably larger than those given by the sigma weight refinement or given by our previous refinements of layer silicates. The positional errors determined for the sigma weighted refinement, for which a slightly larger $R_w = 6.4\%$ was obtained, are comparable to those obtained in our other refinements and are the ones presented here. There were no significant differences in atomic coordinates in the two refinements.

Near the end of the refinement process, difference electron density (DED) sections were flat at all atomic positions. An extra maximum was located just above the OH group on the side toward the interlayer Ba. Although the peak is in the position expected for the H^+ proton of the OH in a trioctahedral mica, the measured electron density of 2.3 units is too large for H^+ alone. The *z*-coordinate of the extra peak is close to that of the crystallographically independent S atom, which because of its large size has its center of gravity appreciably out of the plane of the apical oxygens and closer to the interlayer Ba. We interpret the extra maximum above the OH is due to substitution of S for OH in 10–15% of the unit cells, but with different *z*-coordinates so that the centers of gravity of OH and S do not coincide along **c**. The extra S masks the position of the H^+ proton, for which an electron density of 0.3–0.5 units is usually found. No attempt was made to refine the position of the extra S, but its scattering contribution is included in the final R_w value.

The final atomic coordinates are listed in Table 2. Table 3 gives the bond lengths and angles calculated from these coordinates.

[1] A table of observed and calculated structure amplitudes can be ordered as Document AM-85-290 from the Business Office, Mineralogical Society of America, 2000 Florida Avenue, N.W., Washington, D.C. 20009. Please remit $5.00 in advance for the microfiche.

Table 3. Calculated bond lengths (Å) and angles (°)

TETRAHEDRA

T(1)						T(2)					
T(1)--O(1)	1.612(4)	O(1)--O(3)	2.711(6)	O(1)--T(1)--O(3)	114.3(2)	T(2)--O(2)	1.782(5)	O(2)--O(3)	2.948(6)	O(2)--T(2)--O(3)	109.9(2)
O(3)	1.614(5)	O(4)	2.711(6)	O(4)	113.8(2)	O(3)	1.819(5)	O(4)	2.946(6)	O(4)	110.1(2)
O(4)	1.625(4)	O(5)	2.645(6)	O(5)	109.5(2)	O(4)	1.813(5)	O(6)	3.051(7)	O(6)	117.8(2)
O(5)	1.628(2)	O(3)--O(4)	2.644(6)	O(3)--T(1)--O(4)	109.4(2)	O(6)	1.782(3)	O(3)--O(4)	2.797(6)	O(3)--T(2)--O(4)	100.7(2)
		O(5)	2.567(7)	O(5)	104.7(2)			O(6)	2.918(5)	O(6)	108.3(2)
		O(4)--O(5)	2.569(7)	O(4)--T(1)--O(5)	104.3(2)			O(4)--O(6)	2.922(6)	O(4)--T(2)--O(6)	108.8(2)
Mean	1.620(2)	Mean	2.641(2)	Mean	109.3(1)	Mean	1.799(2)	Mean	2.930(2)	Mean	109.3(1)

INTERLAYER CATION

Ba--O(3)	3.085(5) (x2)	3.250(5) (x2)
O(4)	3.088(4) (x2)	3.191(5) (x2)
O(6)	2.970(7)	
O(6)	3.028(7)	
O(5)	3.270(10)	
O(5)	3.233(10)	
S	3.198(2)	

Mean of all 13 contacts = 3.148(2)

OCTAHEDRA

M(1)		M(2)		M(3)		M(4)	
M(1)--O(1)	2.109(4) (x4)	M(2)--O(2)	2.123(4) (x4)	M(3)--O(1)	2.246(4) (x2)	M(4)--O(1)	2.179(4) (x2)
OH	2.073(5) (x2)	S	2.463(2) (x2)	O(2)	2.032(4) (x2)	O(2)	2.076(4) (x2)
				S	2.407(2) (x2)	OH	2.105(3) (x2)
Mean	2.097(2)	Mean	2.236(1)	Mean	2.228(2)	Mean	2.120(2)
Unshared Edges M(1)		Shared Edges M(1)		Unshared Edges M(3)		Shared Edges M(3)	
O(1)--OH	3.093(5) (x4)	O(1)--OH	2.816(6) (x4)	O(1)--S	3.251(3) (x2)	O(2)--S	3.232(4) (x2)
O(1)--O(1)	3.091(6) (x2)	O(1)--O(1)	2.872(8) (x2)	O(1)--O(2)	3.082(5) (x2)	O(2)--O(1)	2.829(6) (x2)
				O(2)--S	3.182(4) (x2)	O(1)--O(1)	2.872(8)
						S--S	3.793(4)
Mean	3.092(2)	Mean	2.835(3)	Mean	3.172(2)	Mean	3.131(3)
M(2)		M(2)		M(4)		M(4)	
O(2)--S	3.270(4) (x4)	O(2)--S	3.232(4) (x4)	O(1)--O(2)	3.240(5) (x2)	O(1)--O(2)	2.829(6) (x2)
O(2)--O(2)	3.209(5) (x2)	O(2)--O(2)	2.778(9) (x2)	O(1)--OH	3.169(5) (x2)	O(1)--OH	2.816(6) (x2)
				O(2)--OH	3.150(3) (x2)	O(2)--O(2)	2.778(9)
						OH--OH	2.721(10)
Mean	3.250(2)	Mean	3.081(2)	Mean	3.186(2)	Mean	2.798(3)

Cation order

The reduction of symmetry from the ideal *C*-centered to Primitive means that atoms near the centers of the (001) faces must be different from those near the cell corners. There are several reasons for this reduction in symmetry:

1. According to refinement of occupancies the M(1) and M(4) octahedra clustered around each cell corner (Fig. 1) in layer 1 are less Fe-rich than the M(2) and M(3) octahedra clustered around the *C*-face center. M(1) = $Mg^*_{0.59}Fe^*_{0.41}$ and M(4) = $Fe^*_{0.89}Mg^*_{0.11}$ if no vacancies occur, whereas M(2) and M(3) are both 100% Fe*. Fe* does not distinguish between Fe and Mn, or their different valencies, and Al is included in Mg*. In layer 2 the clusters retain their identities, but exchange positions due to operation of the *n*-glide planes parallel to (001) at $z = 1/4$, 3/4 and/or operation of the 2_1 screw axes parallel to [100] at $y = 1/4$, 3/4; $z = 1/4$, 3/4.

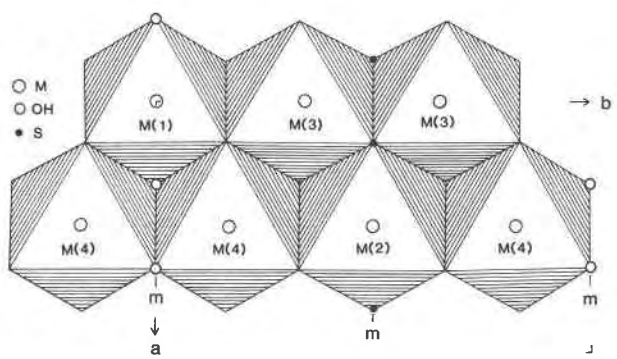

Fig. 1. Octahedra within the first layer of anandite-2*Or*. Sulfur is preferentially associated with the Fe-rich M(2) and M(3) octahedra.

2. Hydroxyl groups are part of the coordination of the Fe-poor M(1)–M(4) clusters near the cell corners, whereas S takes the place of OH in the Fe-rich M(2)–M(3) clusters near the face center.

3. Mean T–O bond lengths and occupancy refinement agree that T(1) = $Si_{1.00}$ and T(2) = $Fe^{3+}_{0.70}Si_{0.30}$, and the total tetrahedral Fe^{3+} so derived agrees with the amount indicated by Mössbauer analysis. Given this ordering, the mirror planes at $y = 0$ and $y = 1/2$ then operate to require adjacent 6-fold rings along **b** to be compositionally and dimensionally different within the same tetrahedral sheet, with 4 T(1) + 2 T(2) in the smaller R1 ring and 2 T(1) + 4 T(2) in the larger R2 ring, as shown in Figure 2. Ring 2 is dimensionally larger than ring 1 along **b**, although the sides along **a** are smaller, and the resultant $b = 9.509$Å is greater than that expected for hexagonal geometry $b = \sqrt{3}a = 9.421$Å. The possible distortional effect of the dimensional differences of these two kinds of rings is diminished by

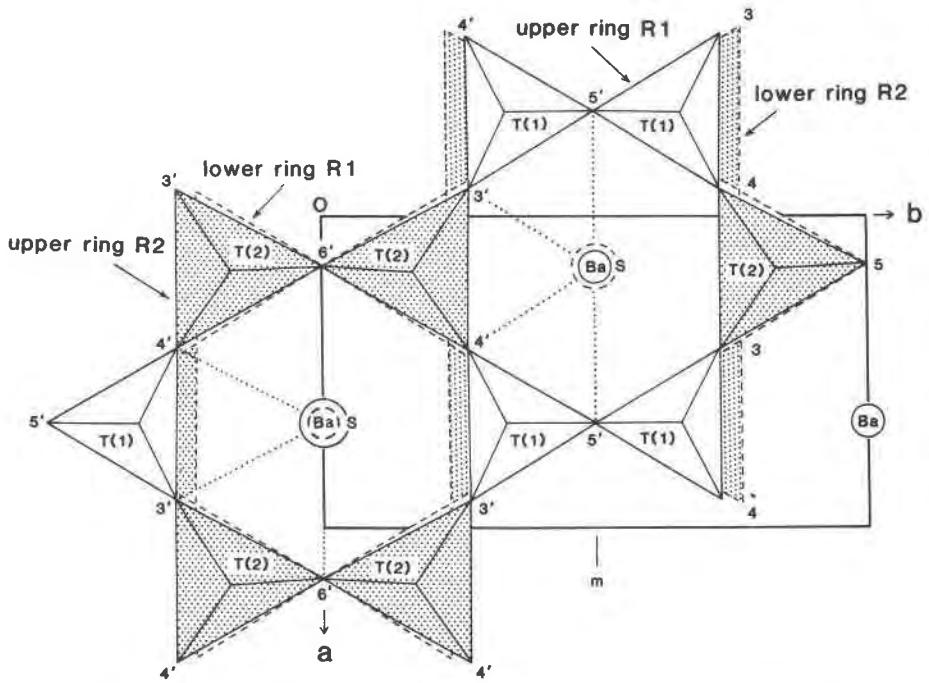

Fig. 2. Non-equivalent 6-fold rings in anandite-2*Or* at junction of layers 1 and 2. Smaller T(1) tetrahedra contain Si only and larger T(2) tetrahedra (dotted) contain a hybrid $Fe^{3+}_{0.7}Si_{0.3}$ cation. Smaller R1 and larger R2 rings face one another across the interlayer gap. S in ring R2 is above Ba on the left and below on the right as a 13th neighbor.

alternating the large and small rings along **c** across the interlayer gap. This alternation is tied into the alternation in position of the Fe-poor and Fe-rich octahedral clusters noted in point (1) above, because the large R2 ring is coordinated primarily to the large M(2) and M(3) octahedra and the smaller R1 ring primarily to the smaller M(1) and M(4) octahedra. Both alternations obey the operation of the symmetry elements of *Pnmn*. The mirror planes create "bow ties" of small T(1) tetrahedra bridged by O(5) atoms and large T(2) tetrahedra bridged by O(6) atoms and thus an ordering pattern quite different than found in other layer silicates where Si and R^{3+} always alternate around all hexagonal rings. If there is an Fe^{3+}-equivalent of the Al-avoidance principle, it certainly is violated in the R2 rings.

The assignment of octahedral compositions in point (1) above is based on refinement of cation occupancies through variation of scattering factor tables and multiplicities plus analysis of DED maps. Interpretation of the Mössbauer pattern by G. A. Waychunas for the octahedra with OH coordination gives 0.39 Fe^{2+} atoms in the *trans* M(1) site (0.41 by refinement) and 0.77 Fe^{2+} atoms in the *cis* M(4) site (0.89 Fe* by refinement, thus suggesting all of the Mn occupies the latter site). The Mössbauer spectrum is extremely complex, probably due to the presence of S and Cl, and there are no analogues for the doublet assignments involving the M(2) and M(3) octahedra. All the octahedral Fe^{3+} must be in these octahedra, however, and this is to be expected because of their linkage to the charge-deficient T(2) tetrahedra. Bond lengths and occupancy refinements suggest that the Cl present by analysis (0.163 atoms) substitutes for S rather than for OH, in accord both with the larger size of Cl and the preference of Mg to avoid Cl in its coordination sphere (Munoz, 1984).

Table 4 summarizes the X-ray and Mössbauer results, and lists our final occupancies for all octahedral cation positions. All Mn has been placed in M(4), Fe^{3+} distributed over M(2) and M(3) in a 2:1 ratio to fit the observed M–O bond lengths, and Al distributed equally over M(1) and M(4). M–O bond lengths calculated for these occupancies, using the effective ionic radii of Shannon (1976), are in very good agreement with those observed (Table 4). Thus, the structural results are internally consistent and agree well with the Mössbauer assignments. There is disagreement with the microprobe analysis, because the structural allocation requires about 0.15 atoms more Fe and less Mg per three octahedral positions than measured by the probe. Probe analysis of the actual crystal used for the structural refinement confirmed the original analysis, so that the error most likely lies in the structural allocation.

The mean bond length of 1.620Å for the T(1) tetrahedron is identical to the value suggested by Smith and Bailey (1963) for pure Si–O in layer silicates but is larger than the 1.608Å value suggested for micas by Hazen and Burnham (1973). It is possible that the small amount of Al found by microprobe analysis (0.10 atoms) is present in T(1) rather than in octahedral coordination, although this would imply either a corresponding increase of Si and decrease of Fe^{3+}

Table 4. Octahedral occupancies and bond lengths

Site	Refinement	Mössbauer	Best Composition	Calc. radius	Calc. M--O	Obs. M--O
M(1)	$Fe^{*}_{0.41}Mg^{*}_{0.59}$	$Fe^{2+}_{0.39}Fe^{3+}_{0.00}$	$Fe^{2+}_{0.40}Mg_{0.53}Al_{0.07}$	0.731Å	2.111Å	2.109Å
M(2)	$Fe^{*}_{1.00}$	-	$Fe^{2+}_{0.70}Fe^{3+}_{0.30}$	0.740	2.120	2.123
M(3)	$Fe^{*}_{1.00}$	-	$Fe^{2+}_{0.83}Fe^{3+}_{0.17}$	0.757	2.137	2.139
M(4)	$Fe^{*}_{0.89}Mg^{*}_{0.11}$	$Fe^{2+}_{0.77}Fe^{3+}_{0.00}$	$Fe^{2+}_{0.81}Mn^{2+}_{0.04}Mn^{3+}_{0.04}Mg_{0.04}Al_{0.07}$	0.749	2.129	2.128

in T(2), contrary to both the occupancy refinement of T(2) and the Mössbauer analysis for total Fe^{3+}, or a small error in the microprobe analysis of Si. Baur (1981) has recently surveyed many silicate structures to arrive at a value of 1.623Å for Si–O, and on this basis we conclude T(1) is occupied by only Si.

It has already been mentioned that both occupancy refinement and Mössbauer interpretation indicate a composition for T(2) of $Fe^{3+}_{0.70}Si_{0.30}$. The mean T(2)–O bond length of 1.799Å is also in close agreement with bond lengths calculated for this composition. The effective ionic radii of Shannon (1976) suggest mean Fe^{3+}–O = 1.870Å in tetrahedral coordination, and linear extrapolation between this value and the Si–O end gives a value of 0.713 Fe^{3+} for T(2) if 1.623Å is used for Si–O and 0.729 Fe^{3+} if 1.608Å is used.

Interlayer region

Ba^{2+} is only slightly smaller than K^{1+} (1.61Å *vs.* 1.64Å for 12-fold coordination) and any changes relative to the K-micas will primarily result from the higher charge and field strength of Ba. For example, in anandite the interlayer gap of 3.083Å between adjacent basal oxygen surfaces is about 0.3Å less than for most K-rich micas. The coordination polyhedron around Ba is asymmetric, because there is a large R2 ring on one side of Ba and a smaller R1 ring on the other side. Ba remains in slightly closer contact with four of the six basal oxygens of the smaller R1 ring (3.085–3.088Å) than with the corresponding four oyxgens of the larger R2 ring (3.191–3.250Å). But due to tetrahedral tilting the Ba is held in pincer fashion by the two shortest bonds (2.970 and 3.028Å) to the two bridging O(6) atoms in ring R2 and by longer bonds (3.270 and 3.233Å) to the two bridging O(5) atoms in ring R1. The mean bond length to all 12 basal oxygens is 3.144Å.

A very interesting feature of the interlayer region concerns the position of the S. The center of gravity of the S is not coplanar with those of the apical oxygens so that the S is deeper within the large R2 ring and closer to the interlayer Ba. Most of this apparent shift of 0.59Å along **c** is due to the larger size of S. Shannon (1976) lists a radius of 1.38Å for oxygen with four cation neighbors and 1.84Å for S^{2-} with six neighbors. Correction for CN = 4 reduces the latter to 1.81Å, so that the centers of gravity of S and O would differ by 0.43Å along **c** if it is assumed that their surfaces are aligned along the octahedral cation plane. Thus the actual shift toward the Ba is 0.16Å. The Ba, in turn, has moved 0.1Å from median plane of the interlayer into the large R2 ring and towards the S. The Ba–S bond length is 3.198Å, which is less than the sum of the effective ionic radii of Ba + S. As a result the S must be considered in contact with and strongly bonded to the Ba as a 13th nearest neighbor. The coordination can be described as an hexagonal prism that is capped on one end. The OH on the other side of Ba within ring R1 is considerably more distant at 4.063Å. The shift of both the Ba and S toward one another is strong evidence that an actual bond exists between them and that S is present as S^{2-} rather than as $(SH)^{1-}$. The good agreement of the observed cation site occupancies and bond lengths for the initial allocation of the chemical analysis based on 23 positive and negative charges, rather than 22, also justifies the latter conclusion. No evidence of an extra electron density maximum attributable to a H^{+} proton could be found on DED maps in the vicinity of the S.

The alternation of octahedral cations between set I and II positions in adjacent layers of anandite-2*Or*, equivalent to alternating 180° layer rotations or alternating + and − directions of intralayer $a_1/3$ shift, leads to a prismatic rather than octahedral coordination of the interlayer Ba by the six nearest basal oxygens. For structures with appreciable substitution of tetrahedral R^{3+} for Si the prismatic coordination normally is considered unstable because it leads to repulsion between unsatisfied charges on opposing basal oxygen surfaces (Takeda et al., 1971). This effect should be especially large for the small interlayer separation found in anandite-2*Or*, but several factors combine to counterbalance the repulsion (Guggenheim, 1984). There is strong attraction between the interlayer Ba^{2+} and the S^{2-} within each layer. The O_b–O_b repulsion is minimized by alternation of the ordering pattern across the interlayer gap so that basal oxygen O(6) unique to the substituted tetrahedron T(2) sits over basal oxygen O(5) unique to the pure Si tetrahedron T(1), and vice-versa. The divalent charge on Ba offsets more of the unsatisfied charges on the basal oxygens than would a univalent cation. And, as discussed

in the next section, corrugations in the basal oxygen surfaces of adjacent layers are in-phase and do not lead to abnormally short contacts across the interlayer gap.

Structural distortions

The angle of tetrahedral rotation (α) measures 0.9° in both rings so that the rings are virtually hexagonal in shape (Table 5). Giuseppetti and Tadini (1972) suggested that the hexagonal shapes of the rings are due to the preference of the divalent Ba to surround itself by as many neighbors as possible, and they calculated by a DLS program that a value of $\alpha = 14°$ would be expected otherwise. This explanation requires revision in view of the refinement of kinoshitalite, another Ba brittle mica, in which an actual tetrahedral rotation value of 12.4° was found by Kato et al. (1979) despite the presence of substantial interlayer Ba. In anandite the small interlayer separation and the observation that Ba is able to slip into the R2 ring by 0.1Å suggest that Ba is not blocking rotation. Although existing equations for calculating the lateral dimensions of unconstrained tetrahedral and octahedral sheets do not take into account the presence of tetrahedral Fe^{3+} or octahedral S^{2-}, the general principles relating to lateral misfit should still apply. We have used the Toraya (1981) equations $b_{tet} = 2\sqrt{3}(e_b)$ and $b_{oct} = 3\sqrt{2}(d_0)$, where e_b = mean observed tetrahedral basal edge length and d_0 = mean observed octahedral cation to anion distance, to obtain an unconstrained b_{tet}/b_{oct} ratio of 1.029 for anandite. Substitution of this value into the regression equation of McCauley and Newnham (1971) gives a predicted rotation angle of 1°, and indicates little lateral misfit of sheets in anandite.

Table 5. Other structural features

Tetradedral rotation (α)	Ring 1	0.9°		
	Ring 2	0.9°		
Tetrahedral angle (τ)	T(1)	112.5°		
	T(2)	112.6°		
Octahedral flattening (ψ)[a]	M(1)	59.8°		
	M(2)	55.3°		
	M(3)	55.2°		
	M(4)	60.2°		
Octahedral distortion				
		internal rms[b]	$(\sigma\theta)^2$	external rms[c]
	M(1)	4.5°	27.4	3.1°
	M(2)	4.3°	25.0	5.6°
	M(3)	7.6°	40.7	6.7°
	M(4)	6.8°	62.3	4.9°
Sheet thickness (Å)	Tetrahedral			2.265
	Octahedral			2.327
	Interlayer separation			3.083
Basal oxygen delta z (Å)	O(5)	-0.13		
	O(6)	+0.18		
Intralayer shift (Å)		$\pm 0.337a_1$		

[a] The mean octahedral angle ψ is defined as: $\cos\psi$ = octahedral thickness/2($\overline{M\text{--}O,OH}$). The ideal ψ is 54.73 degrees.

[b] Rms octahedral distortion as defined by Dollase (1969) is the rms deviation of the 15 bond angles about the cation from their ideal values. $(\sigma\theta)^2$ is defined by Robinson et. al. (1971) as: $(\sigma\theta)^2 = \sum_{i=1}^{12} (\theta_i - 90)^2/11$ where θ_i is the observed O--M--O angle.

[c] Rms octahedral distortion parameter of 36 external octahedral face angles about the anions from their ideal values. Twenty-four of these angles are ideally 60° and 12 are ideally 90°.

The basal oxygens in anandite are corrugated in an unusual pattern as a consequence of tetrahedral tilting and distortion around the *trans* M(1) and M(2) octahedra. Corrugations due to tetrahedral tilting across the large *trans* M(1) vacant site are always observed in dioctahedral layer silicates, but the resulting pattern can be described as a rectified wave in which the wave troughs in a given basal oxygen surface point in the same direction. An alternating wave is observed in anandite with both crests and troughs along the same surface. This is only possible in a Primitive cell, and ideally requires the corner and pseudo *C*-centered octahedra to be of different sizes relative to their coordinating tetrahedra.

The average Si–Si distance taken from the literature for talc, pyrophyllite, and four micas having only Si in tetrahedral coordination is 3.018Å. The unshared lateral edge of the M(1) octahedron, calculated from the Toroya (1981) regression equation using observed M–O distances and ψ flattening parameters, is ideally O(1)–O(1) = 3.146Å. Thus in anandite-*2Or* the ideal lateral edge of the corner *trans* M(1) Fe, Mg octahedron is larger than the ideal distance between coordinating apical O(1) oxygens of the pure Si T(1) tetrahedral "bow tie". Accordingly, in the lower tetrahedral sheet with the tetrahedra pointing up, the O(1) apical oxygens move apart to fit the larger M(1) edge and the bridging basal oxygen O(5) buckles upward to tilt the T(1) "bow ties" across M(1). In the upper tetrahedral sheet O(5) buckles downward. The observed O(1)–O(1) distance of 3.091Å is intermediate between the ideal tetrahedral Si–Si and octahedral O(1)–O(1) values derived above.

Interpretation of the T(2) and M(2) relationship is less straightforward. The ideal T(2)–T(2) distance is unknown for its hybrid $Fe^{3+}_{0.7}Si_{0.3}$ composition, but presumably is somewhat less than the observed value of 3.170Å. Use of the Toraya regression equation yields an ideal lateral edge O(2)–O(2) = 3.180Å in the 100% Fe M(2) octahedron, although the validity of the equation for a partly S-coordinated octahedron is not known. The available evidence thus suggests that the ideal lateral edge of the M(2) octahedron is larger than the ideal distance between coordinating apical O(2) atoms on the T(2) tetrahedral "bow ties", so that the latter should tilt in the same fashion as the T(1) pair. It is observed that the apical O(2) oxygens do spread apart to fit the larger M(2) lateral edge, as expected. This direction of movement also minimizes repulsion between the adjacent S^{2-} anion and the O(2) anions, which are undersaturated due to Fe^{3+} substitution for Si^{4+}. For normal out-of-plane tilting the bridging basal oxygen O(6) would be expected to buckle upward in the lower tetrahedral sheet, similar to O(5), but instead it buckles downward. This anomalous behavior is attributed to attraction between the interlayer Ba^{2+} cation and the undersaturated O(6) anions, whereby Ba is held by the two shortest contacts of its coordination group in pincer fashion by a pair of O(6) atoms. The movements of O(6) and O(2) also require a tilting of the basal edge O(3)–O(4) so that the latter two atoms are not coplanar in (001).

Elevation of the bridging O(5) basal oxygen across the

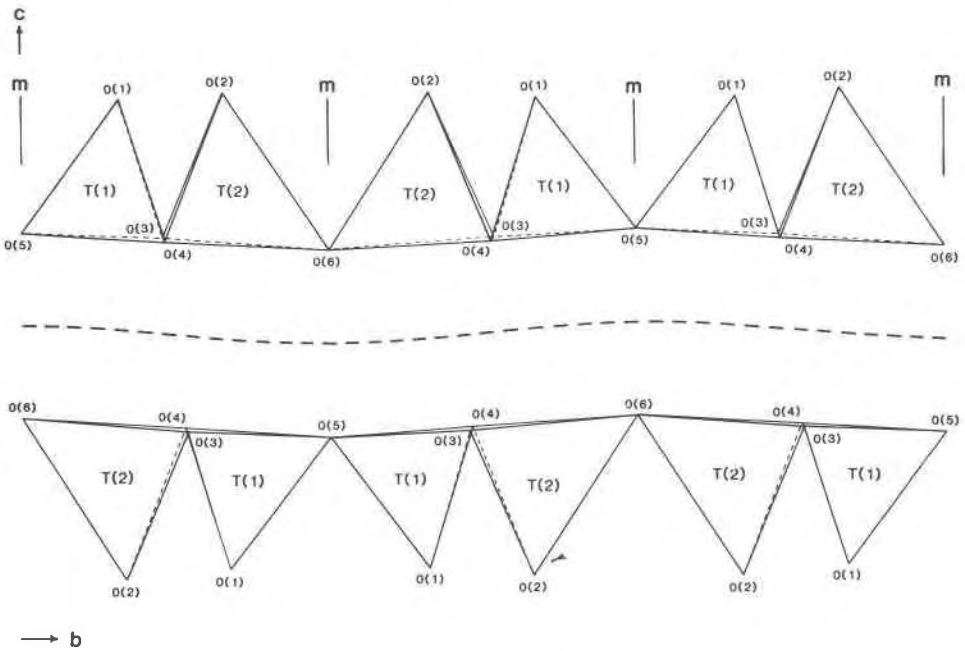

Fig. 3. Alternating wave forms in the basal oxygen surfaces at junction of layers 1 and 2. Alternation of the ordering patterns in the layers keeps the waves in-phase and prevents short O(5)–O(5) and O(6)–O(6) contacts across the interlayer gap.

corner *trans* M(1) octahedron and depression of O(6) across the pseudo *C*-centered *trans* M(2) sets up the alternating wave form illustrated in Figure 3. Individual crests and troughs of the waves run along the mirror planes parallel to the direction of intralayer $a/3$ shift and to the "bow tie" stripes of the R1 and R2 rings, and the amplitudes of the wave forms [−0.13Å for O(5) and +0.18Å for O(6)] shorten the tetrahedral sheet dimension along **b** by 0.2%. The wave forms are in-phase across the interlayer gap, crest-to-crest and trough-to-trough, because the layers are transposed so that the O(5) trough at the top of layer 1 is adjacent to the O(6) trough at the bottom of layer 2; the similar relationship exists for the crests. This correspondence prevents short O(5)–O(6) contacts across the gap and thereby minimizes anion–anion repulsion due to unsatisfied charges on the basal oxygens in the hexagonal prism coordination. The interlocking nature of the waves is only possible in the 2*Or* structure, because this geometry requires intralayer $a/3$ shifts in all layers to be parallel plus a 2-layer structure in which the ordering pattern and wave forms in layer 2 are shifted by the *C*-centering vector relative to layer 1. The combination of the observed ordering pattern and the interlocking wave forms are considered the primary reasons for the stability and the abundance of the 2*Or* structure type in anandite of this composition.

The movement of bridging oxygens O(5) and O(6) noted above is achieved only at the expense of distortions of the T(1) and T(2) tetrahedra. Examination of O_a–T–O_b angles in Table 3 shows that the angle involving O(5) within the T(1) tetrahedron is 4–5° smaller than the angles involving the other basal oxygens O(3) and O(4), whereas the angle involving O(6) within the T(2) tetrahedron is about 8° larger than those involving O(3) and O(4). At the same time T(1)–O(5) = 1.628Å is the longest of the T(1)–O_b bonds, paralleled by shorter O_b–O_b and O_a–O_b bonds involving O(5), and T(2)–O(6) = 1.782Å is the shortest of the T(2)–O_b bonds, paralleled by longer O_b–O_b and O_a–O_b bonds involving O(6).

The large size of S and its shift toward Ba distort the shapes of the M(2) and M(3) octahedra to which the S is coordinated. This shows up best in the octahedral flattening parameter (ψ) and the deviation of the 36 octahedral face angles from their ideal values (termed the external distortion in Table 5). Although the cation to oxygen distances are similar within all four octahedra (Table 3), the cation to cation distances are not uniform. Those within the M(2)–M(3) cluster are shorter by 0.05–0.31Å than those within the M(1)–M(4) cluster. This is due to increase in length of the octahedral shared edges involving S in the M(2)–M(3) cluster. The shortest distance M(3)–M(3) = 2.965Å is across the longest shared edge (S–S = 3.793Å), the second shortest distance M(2)–M(3) = 3.097Å is across the second longest shared edge [S–O(2) = 3.232Å], and the larger M–M distances (3.148–3.272Å) are across the shortest O–O and O–OH shared edges (2.778–2.872Å) that do not involve S. The difference in z parameter of S relative to O(1) and O(2) shows up in the angle between anions within the M(2) and M(3) octahedra. Angles with S at the vertex are all less than 60° [M(2): 50.6–59.5°; M(3): 51.7–57.2°] and those with an apical oxygen at the vertex are mostly greater than 60° [M(2): 60.2–65.4°; M(3): 56.6–72.5°].

Because of their iron- and sulfur-rich compositions, the tetrahedral and octahedral sheets of anandite are unusually thick. Tetrahedron T(1) ideally should be 2.157Å thick for

its pure Si composition, but is extended to 2.232Å. Fe^{3+}-rich T(2), which ideally should be 2.396Å, is thickened to 2.474Å and would be even thicker were it not for shortening of the bond from T(2) to the undersaturated apical O(2) (Table 3). The average tetrahedral sheet thickness is 2.353Å, or 2.265Å if OH and S are included as components of the apical plane (Table 5). The octahedral sheet of ideal thickness 2.531Å is thinned to 2.327Å, but this value is still larger than that of any other mica presently in the literature (Bailey, 1984, Tables 1–2; Guggenheim, 1984, Table 3). The *trans* M(1) and M(2) octahedra lie on centers of symmetry and are constrained not to have counter-rotation of the upper and lower anion triads, but the *cis* M(3) and M(4) octahedra have small rotations of 0.5° and 0.3°, respectively.

Thermal ellipsoids

The equivalent isotropic B values are listed in Table 2. The values are similar for all M cations. The values for T(2) and O(2) are larger than those for T(1) and O(1), as expected from the substitutions in T(2). The values for the basal oxygens likewise are large, as expected from the T(2) substitutions. B_{eq} for O(5) on the mirror plane is exceptionally large (3.95).

The orientations of the anisotropic thermal ellipsoids are listed in Table 6. The major axes of the ellipsoids in general are in the (001) plane along **a** or **b**. The major exception is that for O(2), which is quasi-parallel to **c**. The minor axes are quasi-parallel to **c**, except for O(2). The orientations of the ellipsoids appear to be influenced considerably by positional disorder, primarily involving the hybrid T(2) cation. The major axis of the ellipsoid for basal oxygen O(6) on the mirror plane between two T(2) tetrahedra is oriented normal to the mirror plane and parallel to the T(2)–T(2) "bow tie", as are those for T(2) and Ba (Fig. 4). The major axis of the ellipsoid for apical O(2) is quasi-parallel to **c**. These orientations are consistent with different sizes of the T(2) cation in different unit cells. By contrast, the major axes of the ellipsoids for T(1), O(1), and O(5) are all parallel to **a**, thus suggesting that the T(1)–T(1) "bow ties" adjust their positions as units along **a** in response to the local T(2) sizes. The orientations of the major and median axes of the ellipsoids for the other basal oxygens O(3) and O(4) are intermediate to **a** and **b** and appear to be affected not only by the size of T(2) but also by variable amounts of tetrahedral tilting and rotation due to that size.

Table 6. Orientations of thermal ellipsoids

Atom	Axis	rms (Å) displacement	Angle (°) with respect to a	b	c
Ba	r1	0.104(1)	89.9(8)	90.0(0)	179.9(8)
	r2	0.158(1)	0.1(9)	90.0(0)	89.9(8)
	r3	0.205(1)	90.0(0)	180.0(0)	90.0(0)
M(1)	r1	0.084(6)	83 (16)	90.0(0)	173 (16)
	r2	0.102(3)	90.0(0)	180.0(0)	90.0(0)
	r3	0.102(5)	90.0(0)	180.0(0)	90.0(0)
M(2)	r1	0.083(4)	101.1(5)	90.0(0)	169 (5)
	r2	0.100(3)	90.0(0)	0.0(0)	90 (0)
	r3	0.121(3)	169 (5)	90.0(0)	79 (5)
M(3)	r1	0.080(3)	79 (7)	90.0(0)	169 (7)
	r2	0.098(2)	11 (7)	90.0(0)	79 (7)
	r3	0.132(2)	90.0(0)	180.0(0)	90.0(0)
M(4)	r1	0.094(3)	91 (10)	90.0(0)	179 (10)
	r2	0.100(2)	90.0(0)	0.0(0)	90.0(0)
	r3	0.108(2)	179 (10)	90.0(0)	89 (10)
T(1)	r1	0.054(5)	90 (3)	93 (3)	177 (3)
	r2	0.098(3)	90 (6)	3 (3)	93 (3)
	r3	0.117(3)	180 (6)	90 (6)	90 (3)
T(2)	r1	0.082(3)	90 (3)	82 (1)	172 (1)
	r2	0.121(2)	5 (3)	94 (3)	91 (3)
	r3	0.143(2)	95 (3)	171 (2)	98 (1)
O(1)	r1	0.059(12)	78 (8)	93 (8)	167 (8)
	r2	0.104(6)	86 (19)	5 (15)	92 (9)
	r3	0.120(7)	167 (10)	87 (19)	102 (8)
O(2)	r1	0.087(9)	29 (13)	70 (12)	110 (8)
	r2	0.112(7)	117 (13)	33 (11)	108 (11)
	r3	0.141(6)	100 (9)	115 (10)	153 (8)
O(3)	r1	0.103(9)	120 (5)	94 (3)	149 (5)
	r2	0.165(7)	137 (5)	119 (5)	62 (6)
	r3	0.223(6)	63 (4)	150 (5)	101 (3)
O(4)	r1	0.084(11)	64 (5)	88 (3)	154 (5)
	r2	0.155(7)	38 (4)	63 (4)	66 (5)
	r3	0.226(6)	65 (4)	153 (4)	80 (3)
O(5)	r1	0.089(5)	90 (2)	90.0(0)	180 (2)
	r2	0.111(10)	90.0(0)	0.0(0)	90.0(0)
	r3	0.360(12)	180 (2)	90.0(0)	90 (2)
O(6)	r1	0.125(12)	84 (16)	90.0(0)	174 (16)
	r2	0.163(10)	6 (16)	90.0(0)	84 (16)
	r3	0.241(8)	90.0(0)	180.0(0)	90.0(0)
OH	r1	0.088(11)	180.0(0)	90.0(0)	90.0(0)
	r2	0.120(0)	90.0(0)	90.0(0)	0 (1)
	r3	0.120(0)	90 (0)	180 (1)	90.0(0)
S	r1	0.089(4)	92 (5)	90.0(0)	178 (5)
	r2	0.117(3)	90.0(0)	0.0(0)	90.0(0)
	r3	0.128(3)	178 (5)	90.0(0)	88 (5)

True symmetry

There are several lines of evidence that suggest the true symmetry of anandite-2*Or* is lower than *Pnmn*.

1. Convergence was achieved at $R_w = 6.4\%$ despite the fact that the crystal used was unusually perfect with no indication of streaking of $k \neq 3n$ reflections, that might suggest stacking errors or interstratification.

2. There are a number of violations of the systematic extinctions required by *Pnmn*, as listed in Table 7. The F_0 values for these reflections (and their Friedel equivalents) are considerably greater than 3σ. The *n*-glide plane normal to [100] in particular appears invalid. The listed violations were also observed in data collected from a second crystal.

3. The thermal ellipsoids of atoms O(6) and Ba on the mirror plane are oriented with their major axes normal to the mirror plane. This suggests that the mirror plane does not exist, at least locally.

4. Bond lengths and bond angles involving the atoms on the mirror plane indicate distortions of the *Pnmn* structure that may require relaxation of the symmetry.

5. Examination of the eight general reflections that should be equivalent reveals a pattern of small deviations from orthorhombic symmetry. Two patterns are evident. Both require monoclinic symmetry $P2_1$—(**a** axis unique for the same cell used for *Pnmn*). There is only one violation of this space group in Table 7. Of the 1074 reflections resulting from merging according to orthorhombic symmetry

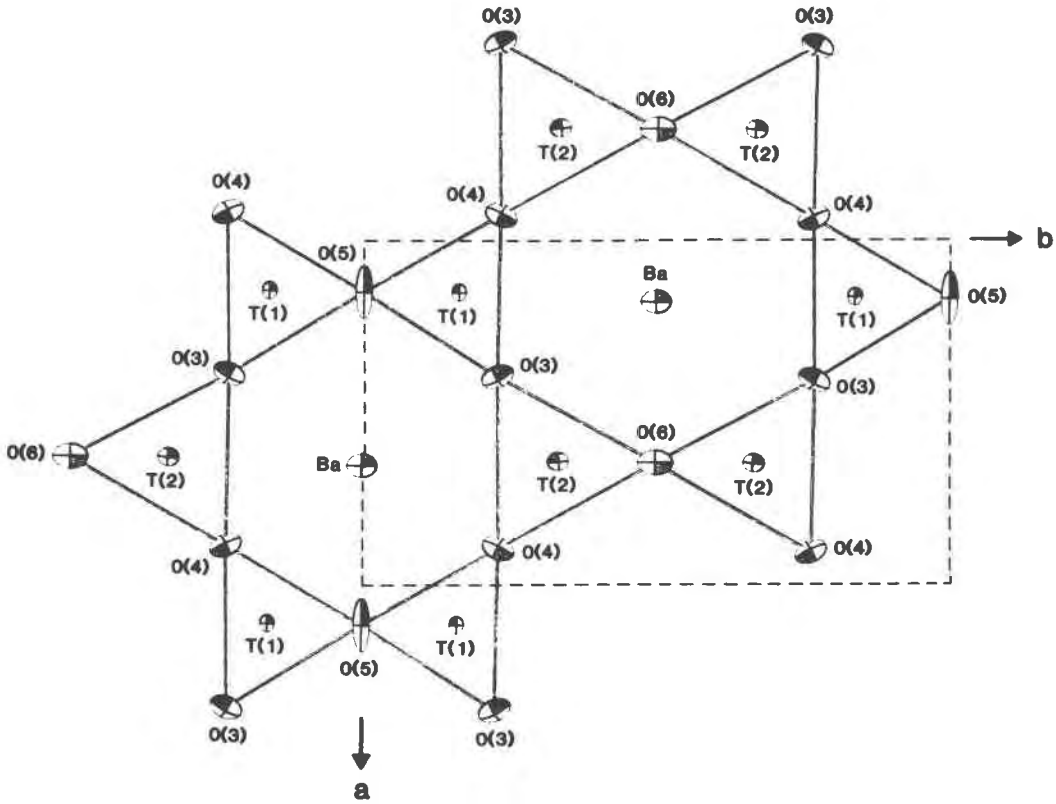

Fig. 4. [001] view of orientations of thermal ellipsoids in layer 1.

approximately 200 show a relationship valid for $P2_1$ with Friedel equivalents equal, so that the structure amplitudes of $hkl = \bar{h}kl = \overline{hkl} = h\bar{k}\bar{l} \neq hk\bar{l} = \bar{h}k\bar{l} = \overline{hk}l = h\bar{k}l$. Another 26 of the reflections were observed as valid for $P2_1$ but with the Friedel equivalents not equal, thus $hkl = \bar{h}kl \neq \overline{hk}l = h\bar{k}l \neq hk\bar{l} = \bar{h}k\bar{l} \neq \overline{hkl} = h\bar{k}\bar{l}$. Both patterns occur primarily, but not exclusively, in reflections with $h + k =$ odd. Because the deviations in general are less than 3σ in both patterns, a second complete data set was collected on a different crystal in order to test the intensity relationships. The resulting observed consistency of the patterns for the same reflections in both data sets suggests a real deviation from orthorhombic symmetry for approximately 20% of the general reflections. We interpret these relationships to signify that most of the structure obeys *Pnmn* on average, but that some atoms do not. The non-equality of the Friedel pairs suggests anomalous scattering and the absence of a center of symmetry for a small part of the structure.

Table 7. *Pnmn* symmetry violations

Violation	Position	h	k	l	F(obs.)	Sigma
2-fold screw	a	3	0	0	11.38	1.84
n-glide	a	0	1	2	13.87	1.37
		0	2	1	15.69	1.00
		0	2	9	22.74	1.28
		0	2	25	36.79	2.95
		0	3	0	17.69	1.34
		0	3	4	10.81	1.50
		0	3	6	27.00	1.03
		0	4	1	19.14	0.86
		0	4	3	33.62	1.10
		0	4	15	50.38	1.80
		0	5	6	18.43	1.12
		0	6	1	31.41	1.27
		0	6	3	31.16	1.25
		0	6	5	37.08	1.27
		0	6	9	19.25	1.50
		0	8	5	31.53	1.27
		0	8	9	33.95	1.33
		0	8	13	33.40	1.52
		0	12	1	33.84	1.76
		0	12	7	31.94	1.63
2-fold screw	b	0	3	0	17.69	1.34
n-glide	c	1	4	0	10.57	1.22
		1	6	0	12.00	1.42
		3	0	0	11.38	1.84
		3	4	0	11.71	1.51

6. Perhaps the most convincing evidence for monoclinic symmetry (a axis unique) comes from the non-orthogonality of the unit cell. Accurate centering of axial reflections with 2θ in the range 84° to 103° yielded crystallographic angles of $\alpha = 90.15(2)°$, $\beta = 90.01(2)°$, and $\gamma = 89.99(2)°$. The non-orthogonality of the α angle was confirmed on four different crystals.

Lowering of the symmetry to $P2_1$ could be due to additional cation ordering involving the T(2) hybrid $Fe^{3+}_{0.7}Si_{0.3}$ cation, although it cannot separate Fe^{3+} and Si completely. Furthermore, additional cation ordering cannot affect the corner M(1) hybrid that is closest to a 50:50 ratio, unless a superlattice exists. Consequently, the lower symmetry is more likely due to distortional effects.

Refinement in $P2_1$ symmetry was attempted by modeling the possible ordering patterns and suspected distortion patterns and by using a DLS program to provide starting atomic coordinates. In the distortion models care was taken to insure that the heavy Ba and S atoms, because of their importance in determining phase angles, were sited off the mirror planes (+ and − in different models). In all cases, however, least-squares refinement of the models gave impossible bond lengths, and DED maps did not provide clues to suggest the nature of the distortion. Refinement was attempted both using all of the data and using only those reflections most sensitive to $P2_1$ symmetry. Friedel "equivalents" were entered as separate reflections, and anomalous scattering factors were used in all refinements.

We conclude that the true symmetry most likely is monoclinic $P2_1$, but that the deviation from orthorhombic *Pnmn* is too small to allow refinement by the methods we have used.

Acknowledgments

This study has been supported in part by National Science Foundation grant EAR-8106124 and in part by Petroleum Research Foundation grant 13157-AC2-C, administered by the American Chemical Society. We are indebted to Dr. Th. G. Sahama of the University of Helsinki for provision of the sample, Dr. E. D. Glover of the University of Wisconsin for the electron microprobe analysis, and Dr. G. A. Waychunas of Stanford University for the Mössbauer analysis.

References

Bailey, S. W. (1980) Structures of layer silicates, Chap. 1 in G. W. Brindley and G. Brown, Eds., Crystal Structures of Clay Minerals and their X-ray Identification, p. 1–123. Mineralogical Society Monograph 5, London.

Bailey, S. W. (1984) Crystal chemistry of the true micas, Chap. 2 in S. W. Bailey, Ed., Micas, Reviews in Mineralogy, 13, 13–60. Mineralogical Society of America, Washington, D.C.

Baur, W. H. (1981) Interatomic distance predictions for computer simulation of crystal structure. In M. O'Keefe and A. Navrotsky, Eds., Structure and Bonding in Crystals, p. 31–52. Academic Press, New York.

Cromer, D. T. and Mann, J. B. (1968) X-ray scattering factors computed from numerical Hartree–Fock wave functions. Acta Crystallographica, A24, 321–324.

Giuseppetti, G. and Tadini, C. (1972) The crystal structure of 2O brittle mica: anandite. Tschermaks Mineralogische und Petrographische Mitteilungen, 18, 169–184.

Guggenheim, S. (1984) The brittle micas. Chap. 3 in S. W. Bailey, Ed., Micas, Reviews in Mineralogy, 13, 61–104. Mineralogical Society of America, Washington, D.C.

Hazen, R. M. and Burnham, C. W. (1973) The crystal structure of one-layer phlogopite and annite. American Mineralogist, 58, 889–900.

Kato, T., Miura, Y., Yoshii, M., and Maeda, K. (1979) The crystal structures of 1M-kinoshitalite, a new barium brittle mica and 1M-manganese trioctahedral micas. Mineralogical Journal (Japan), 9, 392–408.

Lovering, J. F. and Widdowson, J. R. (1968) Electron-microprobe analysis of anandite. Mineralogical Magazine, 36, 871–874.

McCauley, J. W. and Newnham, R. E. (1971) Origin and prediction of ditrigonal distortions in micas. American Mineralogist, 56, 1626–1638.

Munoz, J. L. (1984) F–OH and Cl–OH exchange in micas with applications to hydrothermal ore deposits, Chap. 12 in S. W. Bailey, Ed., Micas, Reviews of Mineralogy, 13, 469–493. Mineralogical Society of America, Washington, D.C.

North, A. C. T., Phillips, D. C., and Mathews, F. S. (1968) A semi-empirical method of absorption correction. Acta Crystallographica, A24, 351–359.

Pattiaratchi, D. B. (1961) Some aspects of the genesis of iron ores in Ceylon. (abstr.) Proceedings 17th Annual Session Ceylon Association for the Advancement of Science.

Pattiaratchi, D. B., Saari, E., and Sahama, Th. G. (1967) Anandite, a new barium iron silicate from Wilagedera, North Western Province, Ceylon. Mineralogical Magazine, 36, 1–4.

Robinson, K., Gibbs, G. V., and Ribbe, P. H. (1971) Quadratic elongation: a quantitative measure of distortion in coordination polyhedra. Science, 172, 567–570.

Shannon, R. D. (1976) Revised effective ionic radii and systematic studies of interatomic distances in halides and chalcogenides. Acta Crystallographica, A32, 751–767.

Smith, J. V. and Bailey, S. W. (1963) Second review of Al–O and Si–O tetrahedral distances. Acta Crystallographica, 16, 801–811.

Takeda, H., Haga, N., and Sadanaga, R. (1971) Structural investigations of polymorphic transition between $2M_2$-, 1M-lepidolite and $2M_1$ muscovite. Mineralogical Journal (Japan) 6, 203–215.

Toraya, H. (1981) Distortions of octahedra and octahedral sheets in 1M micas and the relation to their stability. Zeitschrift für Kristallographie, 157, 173–190.

Manuscript received, December 5, 1984;
accepted for publication, July 22, 1985.